analysis, run at various stages of the recharge process, showed a progressive attenuation of the Cu and Li_2S reflections, followed by the formation of a complex mixture of sulfides (*e.g.*, $Cu_{1.96}S$, Cu_2S, $Cu_{1.8}S$, CuS).

The rather complicated oxidation mechanism for the Li/Cu_2S system excludes any immediate application of this system in secondary lithium batteries.

Acknowledgments

We acknowledge the support of the Consiglio Nazionale delle Ricerche (CNR) for this research.

Manuscript submitted Oct. 14, 1983; revised manuscript received Nov. 2, 1983. This was Paper 75 presented at the Washington, DC, Meeting of the Society, Oct. 9-14, 1983.

The University of Rome assisted in meeting the publication costs of this article.

REFERENCES

1. B. Scrosati, B. Di Pietro, F. Bonino, M. Lazzari, and G. Razzini in "Power Sources for Biomedical Implantable Applications and Ambient Temperature Lithium Batteries," B. B. Owens and N. Margalit, Editors, Vol. 80-4, p. 276, The Electrochemical Society Softbound Proceedings Series, Pennington, NJ (1980).
2. F. Bonino, L. Busani, M. Lazzari, M. Manstretta, B. Rivolta, and B. Scrosati, *J. Power Sources*, **6**, 261 (1981).
3. M. Lazzari, G. Razzini, B. Rivolta, F. Alessandrini, and B. Scrosati in "Lithium Batteries," H. V. Venkatasetty, Editor, Vol. 81-4, p. 21, The Electrochemical Society Softbound Proceedings Series, Pennington, NJ (1981).
4. M. Boccoli, F. Bonino, M. Lazzari, and B. Rivolta, *Solid State Ionics*, **7**, 65 (1982).
5. F. Bonino, M. Lazzari, and B. Scrosati, *This Journal*, In press.
6. F. W. Dampier, *ibid.*, **121**, 656 (1974).
7. J. P. Gabano, V. Dechenaux, G. Gerbier, and J. Jammat, *ibid.*, **119**, 459 (1972).

Electron Microscopy Study of Formation of Thick Oxide Films on Ir and Ru Electrodes

V. Birss,*,[1] R. Myers, H. Angerstein-Kozlowska, and B. E. Conway*

Department of Chemistry, University of Ottawa, Ottawa K1N 9B4, Ontario, Canada

ABSTRACT

The thick (5-60 μm) oxide films that can be formed electrochemically at Ir and Ru electrodes are examined by scanning and transmission electron microscopy. Their morphologies are discussed in relation to the remarkable reversibility of redox processes associated with the thick films and the enhancement of apparent electrocatalytic effectiveness of the oxide films, which is found for anodic Cl_2 and O_2 evolution processes to increasing extents with growth of the oxide film. The latter effects are much larger at Ir than at Ru. This difference is likely to be associated with the different morphologies of electrochemically grown oxide films that are observable on these two metals. In the case of Ir, the apparent enhancement of electrocatalysis for anodic Cl_2 or O_2 evolution seems to be associated with development of a hyperextended, microporous, hydrous oxide film that is accessible to H_2O and Cl^- ions. Comparisons are made with thermally formed oxide films generated by decomposition of $RuCl_3$ coatings.

The formation of oxide films on noble metals has been the subject of a large number of papers on account of the interest of this topic for (*i*) electrocatalysis of organic molecule oxidations (1-3), anodic Cl_2 evolution (4-6), and O_2 reduction (7), and (*ii*) as a model-type system for studying the transition from monolayer oxide film formation to development of multilayer oxide phases (8-10) on metals. The states of thick oxide films on Ir and Ru, where the oxides are principally IrO_2 and RuO_2, respectively, are of particular interest in relation to electrocatalysis for Cl_2 evolution as treated in previous papers from this and other laboratories.

Much of the earlier work was concerned with the mechanisms and characteristics of formation of monolayer films of OH and O species on Pt and Au, and the resolution of the reversible from the irreversible stages of the oxide film formation processes at the submonolayer level of coverage. [For review, see Ref. (3).]

The growth law for potentiostatic oxide film extension at Pt was established by Gilroy and Conway (11) as the direct logarithmic one in time, even at submonolayer levels of surface oxide formation, and a possible mechanism for this behavior was treated by Gilroy (12). Applications of the Mott-Cabrera "high field" growth mechanism (13), which applies to development of thicker insulating dielectric films, were made by Ord and Ho (8), by Damjanović *et al.* (9, 10), and in related ways by Vetter and Schultze (14).

The first indication that the oxide film formation and growth process at Ir is different from that at Pt or Au was given in the work of Stonehart *et al.* (15), who showed that surface oxide formation and reduction at Ir behaves as a reversible process which can also be observed as optically (16) reversible. Subsequently, a number of papers appeared characterizing this "reversible" type of oxide film behavior; in particular, Gottesfeld *et al.* (17) showed that the reversible behavior is not associated with metal oxidation and reduction of oxide back to the metal, but rather the oxide remains on the surface throughout a cyclic variation of potential between 0.0 and 1.4 E_H, but a redox process takes place within the film. The transition between true OH/O monolayer formation and reduction at Ir and development of thicker films was recently studied by Mozota and Conway (18).

Following the work on Ir (15, 18, 19, 20), similar behavior was found at Ru by Hadzi-Jordanov *et al.* (21) in this laboratory and by Rand *et al.* (22), and the transition from monolayer oxide formation and reduction to reversible redox behavior at oxide films formed at Ru either thermally or by potential cycling was demonstrated in the work of Hadzi-Jordanov *et al.* (21). Since that time, Burke (23) has shown that similar behavior can be generated at several other metals, even Rh and Pt, by a potential cycling regime.

By extensive cycling at Ir and Ru, optically and electron optically visible oxide films can be generated and their morphologies examined and related to their electrochemical behavior, *e.g.*, electrocatalysis for Cl_2 (24) or O_2 (25, 26) evolution reactions. This paper reports scanning electron microscopy studies on such oxide films. Elsewhere (30), we report XPS results on the electronic states of Ir and O in electrochemically formed oxide films at Ir.

* Electrochemical Society Active Member.
[1] Present address: Department of Chemistry, University of Calgary, Calgary, Alberta, Canada.

Experimental

Electrodes.—High purity-grade (Materials Research and Engelhard) Ir rod or wires were employed as the Ir electrode materials. The 4 mm diam rod was cut into 0.5 mm thick circular sections and spot-welded to an Ir wire that was presealed into a soft-glass tube as electrode holder. Ir wire electrodes were spot-welded to a very short length of fine Pt wires presealed into glass tubes. The purpose of this procedure is to avoid preoxidation of Ir, which can occur under flame treatment. Zone-refined Ru rods were also obtained from Materials Research Company, cut, and similarly mounted or directly sealed into glass tubes. Ru wire was not obtainable.

Solutions.—1.0 or 0.5*M* aqueous H_2SO_4 solutions used in the work were prepared from Cl^--free BDH Aristar grade sulfuric acid; in our experience, this is the best grade of this acid available from the point of view of purity. Pyrodistilled water (27) was used for preparation of all solutions, and high purity techniques were employed in all the electrochemical experiments, as reported elsewhere (18, 24, 27).

Types of experiments.—Oxide films were generated on Ru and Ir electrodes by a potential-cycling regime [*cf.* Ref. (18-21)] using an anodic potential limit of at least +1.4V and a cathodic limit of +0.05V E_H. Potentials were referred to that of an H_2 reversible electrode in the same solution (scale designated "E_H, V"), but in a separate compartment of a three-compartment cell. The potential cycling regime was established by means of a cyclic voltammetry setup employing a Wenking potentiostat and a function generator in the usual way. The counterelectrodes were always made of the same metal, Ru or Ir, as that used as the respective test electrode in order to avoid contamination by a foreign metal, *e.g.*, from a Pt counterelectrode by dissolution [*cf.* Ref. (28)].

In some experiments, potentiostatic oxide film formation was investigated. As found previously (15), the oxide film on Ir cannot be grown in time by holding the potential constant at an appropriate value, 1.4 ~ 1.6V E_H; only under a cyclic-potential program does it grow. However, the oxide film at Ru can be grown either by the cycling regime or under constant potential conditions, *viz.*, at > 1.45V, E_H, with the growth rate increasing with higher anodic potentials.

During the course of the growth of the film on Ir, the now well-known electrochromic effect (29) is observed, provided the extent of oxide film thickening is not too great (18), when the film becomes black at all potentials. Ru also showed some electrochromic effect in alkaline solution, but this is less marked than that at Ir.

During the oxide film-formation process, either at Ir or Ru, some dissolution of the metals occurs giving brownish solutions after prolonged cycling. The dissolution (at Ru) is greater under cycling conditions [*cf.* Ref. (28)] than under steady anodic polarization.

In another set of experiments, growth of the oxide was carried out at Ru under constant current conditions or under the influence of a program in which the current was increased from 0.1 to 5 mA cm^{-2} over 4h. The extent of growth of the oxide film under constant current conditions for 4 ~ 5h was found to be equivalent to that under potential cycling (0.05 to 1.45V, E_H) over a period of 3 ~ 4 days. Of course, in a potential cycling regime, the fraction of time spent in each half-cycle over the potential range where oxide growth rate is significant, will only be *ca.* 20%. Under controlled current conditions, however, O_2 gas is evolved so that the film growth partial current is a small fraction of the overall current passing. If O_2, rather than Cl_2 [*cf.* Ref. (24)], is evolved at oxidized Ir electrodes, the oxide film suffers mechanical degradation. This does not occur when Cl_2 is evolved.

Scanning electron and optical microscopy.—A "Semco" Nanolab 7 scanning electron microscope was employed to study the morphology of the oxide films up to high magnifications using a LaB_6 filament. Photomicrographs were taken at various tilt angles which illustrated three-dimensional aspects of morphologies. The oxides of Ir or Ru generated in these experiments did not require coating by C or Au as they were already quite conducting.

Optical microscopy observations were also made using a Nomarski interference microscope.

X-ray emission analyses.—The SEM was fitted with Microspec wavelength and Kevex energy dispersive x-ray analyzer systems, which enabled elemental compositions of materials to be monitored during SEM.

O:Ru and O:Ir ratios were evaluated using the x-ray spectrometers attached to the SEM. The oxygen:metal ratios were determined on various samples of oxidized Ru or Ir by reference to thermally formed bulk standard materials (RuO_2 and IrO_2). The Ru count rate was determined on the electrochemically formed oxide film at Ru and compared with that from the RuO_2 standard. Similar measurements were made on oxidized Ir electrodes.

Morphology and electrochemical history.—Photomicrographs were taken on oxide films grown to various thicknesses. Each sample was characterized by a cyclic voltammogram taken just before the electrode was transferred, after a brief wash in pyrodistilled water, to the SEM chamber. With some electrodes, a cyclic voltammogram was taken also immediately after the electron micrography to check if any irreversible changes had occurred on account of the electron microscopy observations, *e.g.*, due to vacuum drying or electron-beam reduction. The cyclic voltammograms for Ru were hardly changed after exposure of the oxide films in the SEM.

The optical microscopy was done on electrodes transferred in the wet state to the microscope stage so that artifact structures that could result from drying at an elevated temperature were avoided.

Several micrographs were made by transmission electron microscopy (TEM) after making replicas by means of collodion treatment. This procedure gave highest levels of magnification up to 25 nm per cm of the printed photographs. In the TEM instrument, electron diffraction characterization of the actual object material could also be made.

"Electrochemical" film thickness.—By means of the cyclic voltammetry measurements, the electrochemically determined apparent film thickness of the oxide films was determined in terms of the ratio, CEF, of the charge under the cyclic voltammogram, $i\ dt \equiv i/s \cdot dV$, for a sweep-rate $s = dV/dt$, for a given oxide film to that for initial true monolayer[2] formation or reduction (18). This ratio was termed the "charge enhancement factor" (CEF) in previous publications (18, 24).

Results and Discussion

Electrochemical characterization of oxide films at Ir and Ru.—Typical cyclic voltammograms showing the transition from monolayer to multilayer oxide film formation at Ir and Ru are shown in Fig. 1 and 2, and illustrate the major difference between the behavior of the two-dimensional surface monolayer processes, which are irreversible, and the reversible behavior of the multilayer films having CEF values up to several hundred (18). The variation in the shapes of the cyclic voltammograms with potential for oxide films formed at Ir (Fig. 1) is principally due to the change of conductivity (31) of the oxide film at Ir as it is reduced from IrO_2 to Ir_2O_3 (29) at potentials < *ca.* 0.65V E_H. In the case of the ruthenium oxide film (Fig. 2), good conductivity is retained throughout the potential range 0.05-1.4V E_H, *i.e.*, down to the H_2 re-

[2]Care must be exercised at Ir or Ru in the evaluation of the true oxide monolayer formation and reduction cyclic voltammogram (18): thus, it is easy for multilayer oxide formation to begin unless the potential limits of the cyclic-voltammogram are carefully controlled and appropriately limited (18). Such effects are seen in some previously published work (30) where monolayer behavior was referred to, but, in fact, the currents correspond to some multilayer redox component processes.

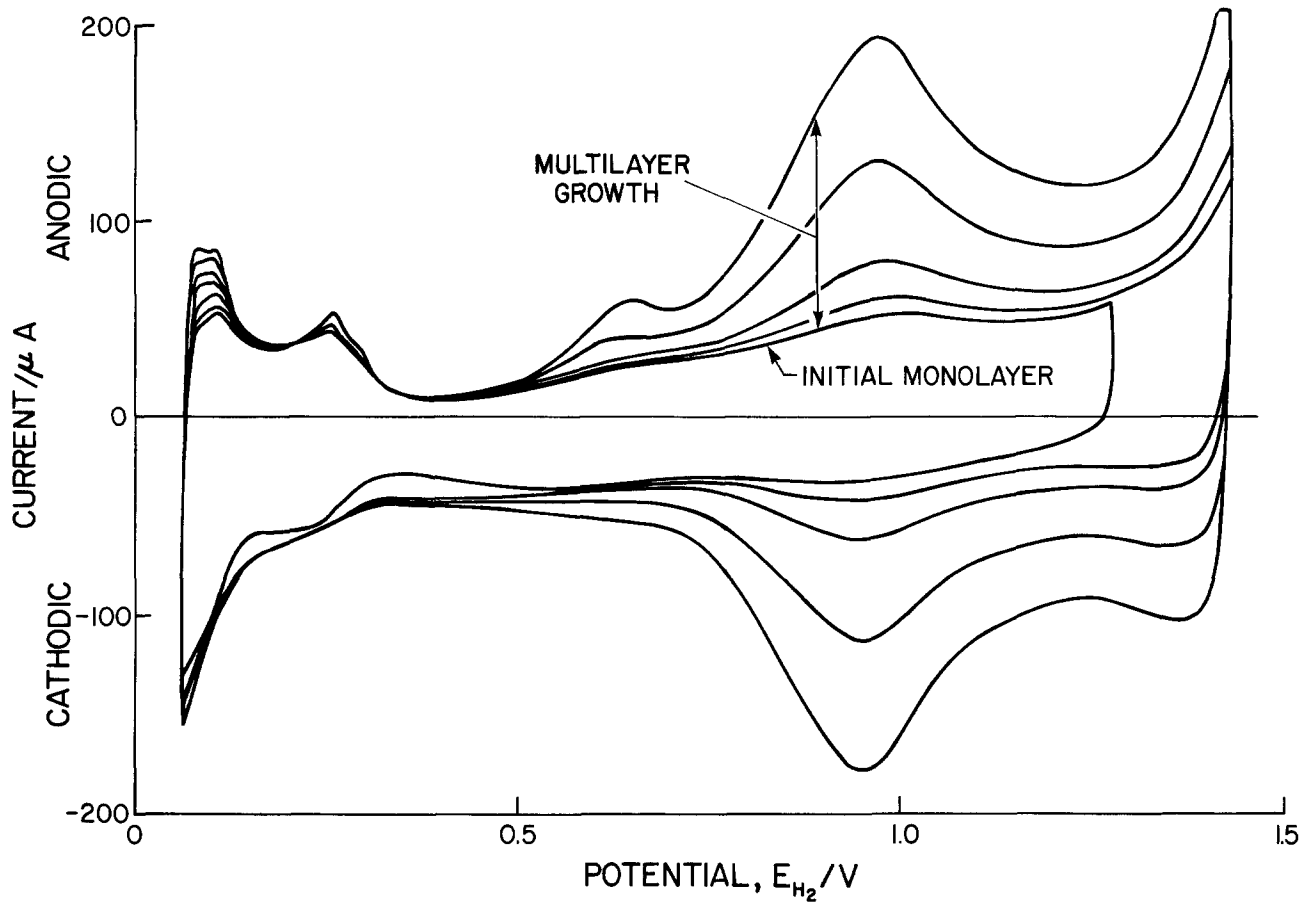

Fig. 1. Cyclic voltammograms for Ir electrode at 295 K showing transition from monolayer oxide film formation and reduction to development of multilayer oxide films with reversible oxidation-reduction region after cycling.

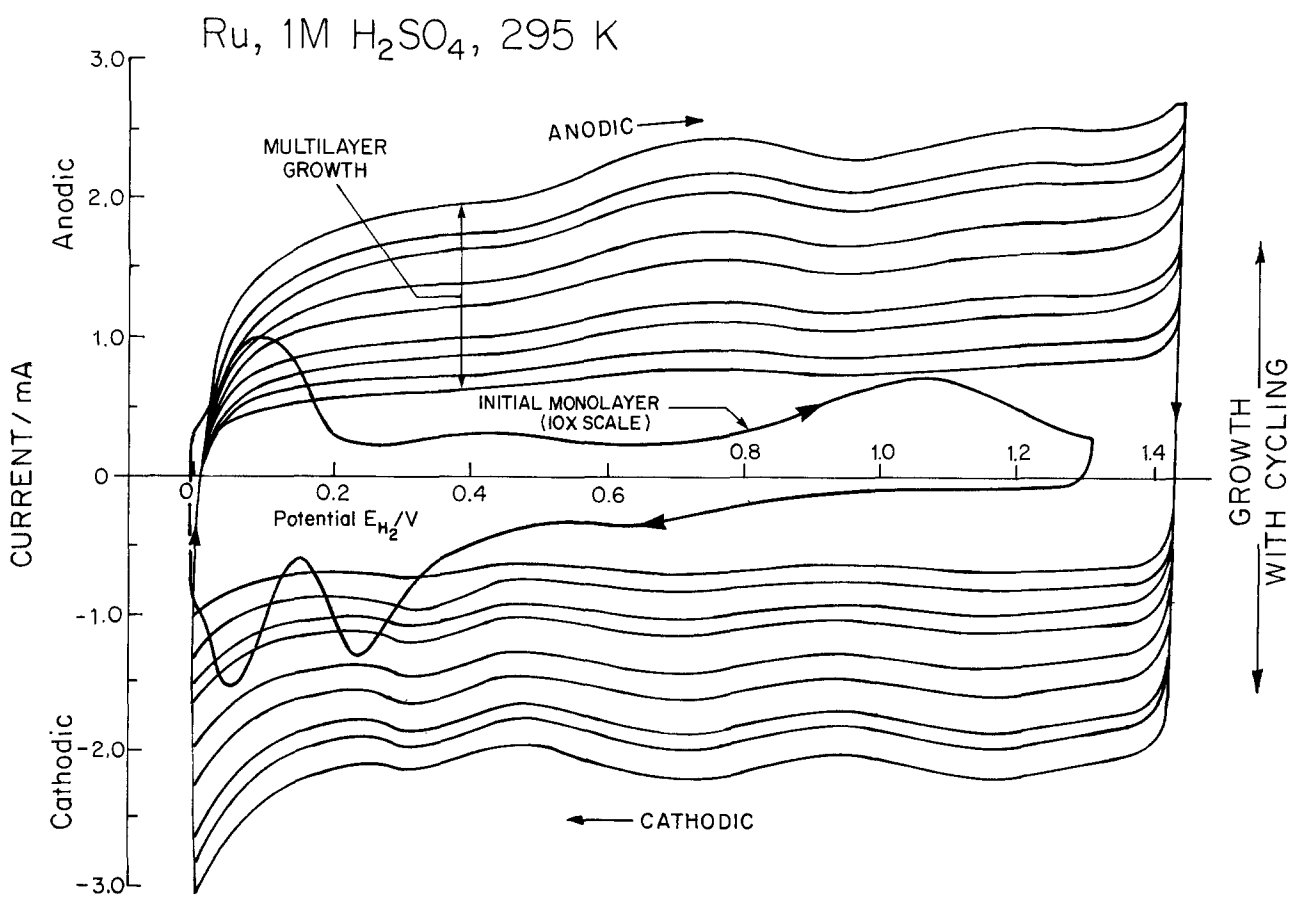

Fig. 2. Cyclic voltammograms for Ru electrode showing monolayer to multilayer oxide film transition, as with Ir shown in Fig. 1

versible potential in the "reduced" state as well as in the oxidized state.

The thicknesses of oxide films estimated from CEF values (based on 0.3 nm per layer, corresponding to passage of charge of 220 μC cm^{-2}) are substantially smaller than are indicated from the dimensions of edges of cracked films that are observed in SEM pictures (see below). A comparison of normalized currents at a given potential (0.8V E_H) in the cyclic voltammograms for Ru and Ir during the growth under cycling conditions, with the film thicknesses observed in the SEM, is shown in Fig. 3. These lines give an approximate idea of the relationship between the effective "electrochemical" thickness of the films and the apparent (*i.e.*, allowing for porosity in the structures) geometrical thickness. The discrepancy is by a factor of *ca.* 10 or more for Ir oxide films and 50-100 for Ru oxide films grown electrochemically. These discrepancy factors may be due to (*i*) microporosity in the hydrous oxide films, and/or (*ii*) limited electrochemical accessibility of the material inside the films, or (*iii*) to electrochemical redox activity being restricted only to the surfaces of pores; that is, the charging/discharging processes observed in cyclic-voltammetry experiments may arise quasi-two-dimensionally at the surface of a hyperextended microporous structure.

Optical interference microscopy observations.—The first microscopic observations of the oxide film on cycled Ru electrodes were made by means of a Nomarski optical interference microscope, with the electrodes still in a wet or damp state. Two photographs of the oxide film developed after *ca.* 200 cycles of potential change from 0.05 to 1.4V E_H are shown in Fig. 4a. This photo shows that the oxidized Ru electrode has a smooth shiny outer surface layer, but the underlying thick film formation cannot be observed in the SEM (see below). After thick film formation has occurred, this smooth outer layer seems to overlay some looser oxide material underneath it (Fig. 4b). The smooth outer layer is extremely hard, as was indicated by its resistance to attempts to probe into it with a steel needle. However, by means of the needle or a scalpel, flakes of this hard oxide layer can be separated off from the underlying bulk Ru oxide or the metal, revealing a looser material beneath. At Ir, such a layer is not observed.

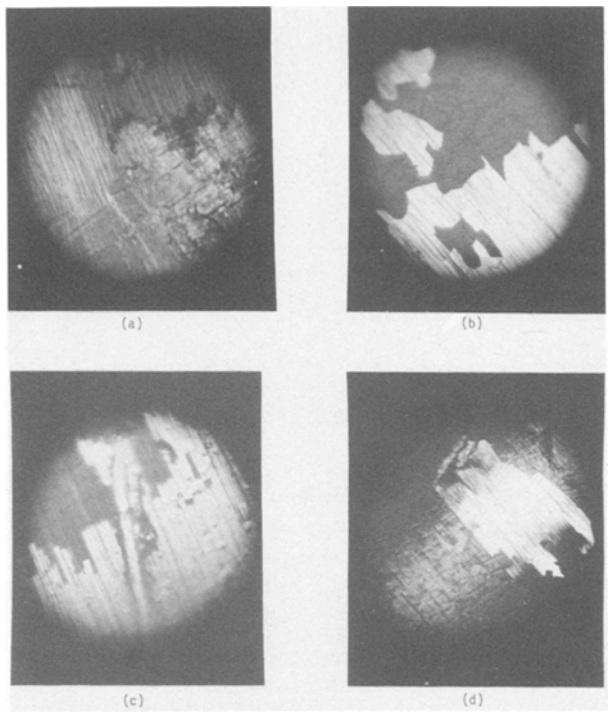

Fig. 4. Nomarski optical microscope photos of the hard shell layer that develops on Ru electrodes as they are oxidized in a potential cycling program. Original photos are Kodachrome showing interference contrast colors of various regions of the surface. a (top left): initial stage of film formation, *ca.* 50 nm. b (top right), c (bottom left), and d (bottom right): thicker films peeling off electrode, *ca.* 5μm.

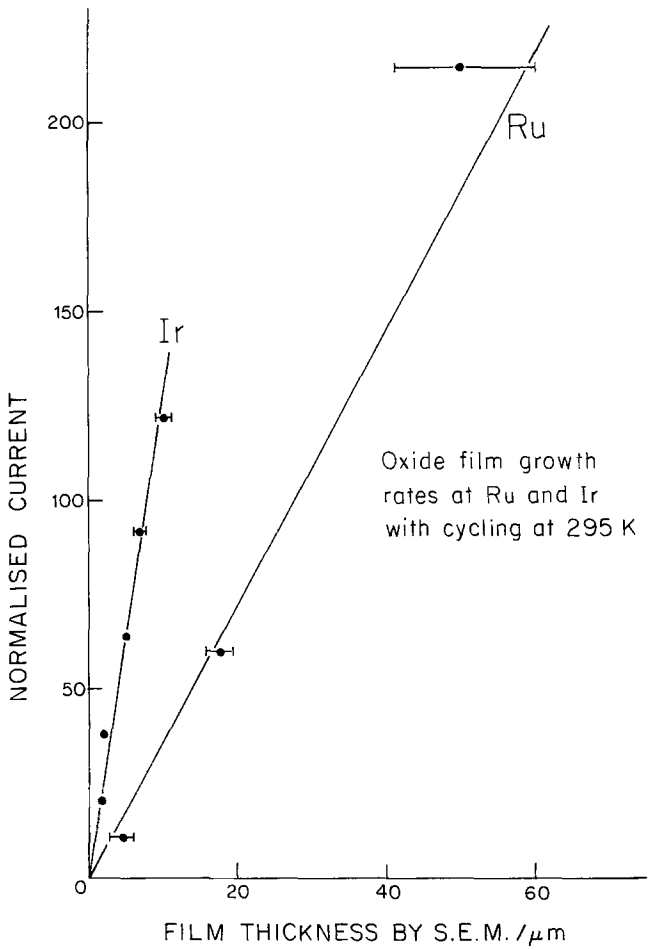

Fig. 3. Relation of normalized currents at 0.8V E_H for Ru and 1.0V for Ir in cyclic voltammograms taken during the oxide film growth during cycling, to film thickness determined by SEM observations. (Normalized currents are approximately proportional to CEF's.) Conditions: 0.5M H_2SO_4, 298 K, cycling between 0.0 and 1.5V E_{H_2} at 0.1 V s^{-1}.

An interesting aspect of the development of the oxide films on Ru is that if the original metal surface is scratched, or otherwise retains some polishing lines, the scratch marks are retained on the outside of the electrochemically grown oxide film. The outer surface of the oxide film, referred to above, has an appearance shown in Fig. 4a and 4b. The retention of the scratch marks indicates that the oxide film grows by migration of OH or O ions into the film rather than the reverse process of metal ion formation and migration outwards (*cf.*, the radioisotope marking procedure of Davies (32) for studying O or metal ion migration processes in oxide-film formation at base metals) coupled with provision of OH^- or O^{2-} species from H_2O at the oxide/solution interface.

More detailed indications of the structure of the oxide films at Ru and Ir are given by the electron microscopical observations to be described next.

Scanning electron microscopy observations.—In this section, we shall describe, first, the general morphology of the oxide films at Ru and Ir as seen with the SEM and then refer more specifically to certain aspects of the morphology of the oxide films, *e.g.*, the presence of columnar structures and the identification of rather small scale porosity.

General morphological features.—The appearance in the SEM of the hard outer layer material, referred to above, is shown in Fig. 5. The persistence of the original scratch marks on the metal, now on the outer surface of

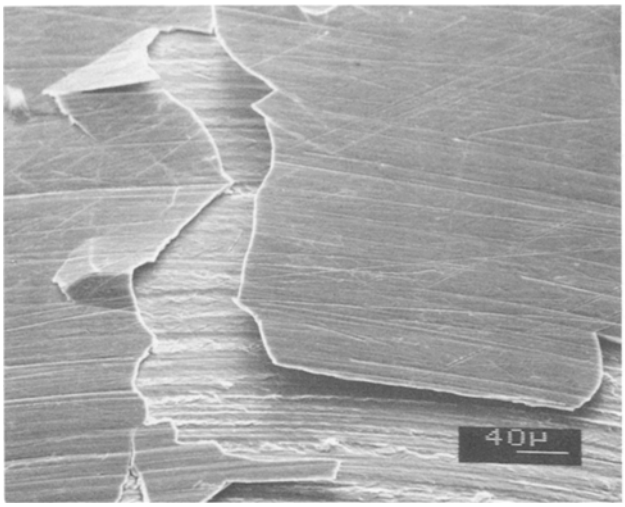

Fig. 5. SEM photos of the hard outer shell layer at an electrochemically oxidized Ru electrode (cf. Fig. 4a and 4b). Note retention of scratch marks.

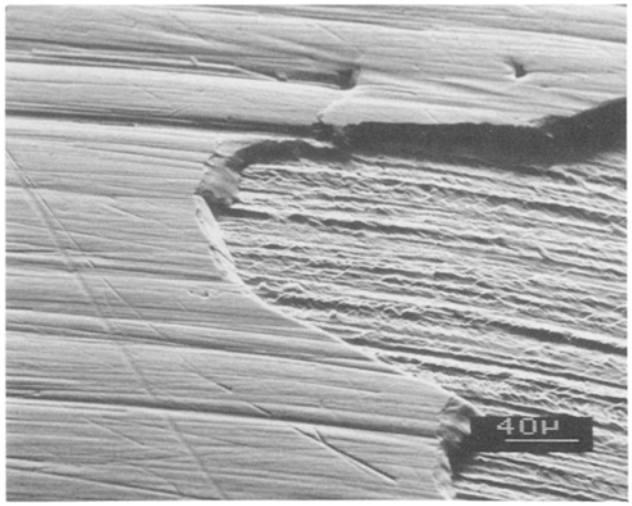

Fig. 7. SEM photo of the oxide film at Ru at high magnification showing edge of a fractured region.

the oxide film, is seen again. At higher magnification, the general appearance of the film is shown in Fig. 6, where the scratch marks are again clearly seen on the outside of the film. Figure 6 shows the structure of the film at a still higher magnification ("4.0 μm" scale) looking into its edge.

Figure 8 shows a region where some oxide has broken away, exposing an underlying oxide or the substrate Ru metal itself. (Compare the optical photomicrographs in section 2, Fig. 4a and 4b). The CEF values for the oxide films shown in the above figures are *ca.* 400. The depth of the depression in Fig. 8 is *ca.* 6 μm, indicating an oxide thickness of at least this magnitude. The CEF was 400 which would correspond only to an "electrochemical thickness" of *ca.* 0.12 μm. This verifies the deduction that the electrochemical charge associated with a change of oxidation state of the film in cyclic voltammetry experiments corresponds to only a small fraction of the oxide film material actually generated by the potential cycling procedure. Alternatively, the film is highly porous or the reversible electrochemical activity originates only at the outer regions of a porous structure.

The oxidation behavior of Ir appears to be significantly different from that of Ru in the following ways. Although a thick oxide film can also be formed, as at Ru, it is only generated by potential cycling, not under constant potential or constant current conditions where

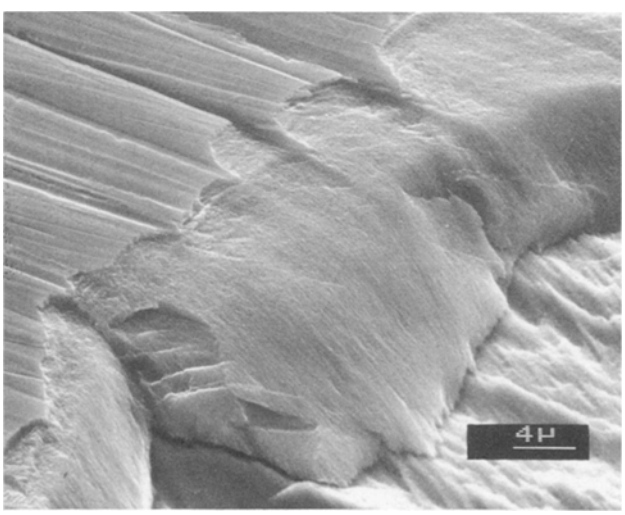

Fig. 6. General appearance of the oxide film at a Ru electrode at higher magnification than that of Fig. 5. Note retention of scratch marks.

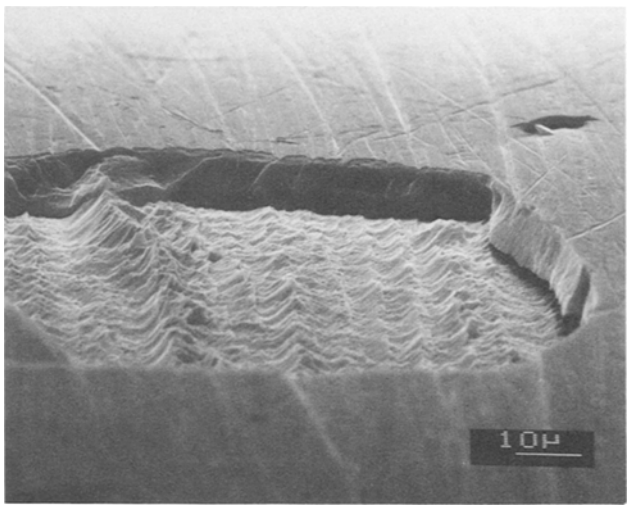

Fig. 8. SEM photo of the oxide layer at Ru showing a region where the film has broken away exposing underlaying material.

Ru will form a thick oxide film. Also, very little dissolution of Ir is detectable, even after several hundred growth cycles; hence Ir oxide film growth is not connected with a dissolution redeposition cycle. This is demonstrated by the independence of growth rate upon electrode rotation (Fig. 9) (0 or 4000 rpm) using an Ir rotating disk electrode. At Ru, by contrast, appreciable metal dissolution takes place during the oxide forming process, as can be seen visually from the gradual coloration of the solutions which became brown.

Figures 10a, 10b, and 10c show the structure of an electrochemically formed oxide film at Ir with a CEF of 180. Again, the thicknesses of the films are substantially greater than corresponds to the CEF value. A cracked structure, similar to dried-out mud, is seen, and, although the oxide film appears to be peeling off in some photos, it was found that electrochemically oxidized Ir electrodes are mechanically stable to Cl_2 evolution for extended periods of time at 100 mA cm^{-2}. Thus, a given electrode does not suffer diminution of CEF by this treatment, though the stability to O_2 evolution is not as good as to Cl_2 evolution.

The "tubular" pore structures found at oxidized Ru (Fig. 11 below) are not observed at Ir although the apparent electrocatalytic behavior (24) for Cl_2 evolution does suggest the presence of a microporous, hyperextended large area structure.

Specific morphological features.—Under certain conditions and/or at high magnifications, several special fea-

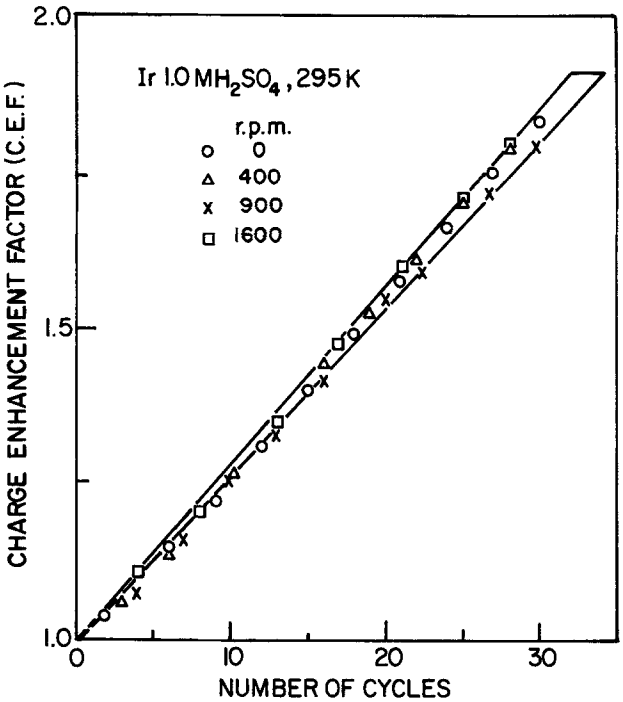

Fig. 9. Independence of anodic currents in cyclic voltammograms for oxidation processes at Ir electrode on electrode rotation rate. CEF's are independent of rotation rate. (Outer lines show breadth of errors; differences at various rotation rates are less than these errors.)

tures of the structure of the oxide films formed on Ru can be observed.

First, Fig. 11 shows the remarkable columnar structure that is seen in a fracture section across the oxide film grown at a fast cycling rate (1 V s^{-1}) to a CEF of *ca.* 200. The photo in Fig. 12 shows this columnar structure at a higher magnification together with top ends of the parallel columns. The orientations of the columnar structures seem to depend on the grain orientation of the original metal or else specific orientations of grains of oxide are developed during the oxide growth, as shown in Fig. 13. As will be discussed later, these columnar structures may result from anodic etching with concurrent oxide film formation at the etched regions, *i.e.*, involving a nonpassivating oxide layer.

An oxide film that has been formed at a Ru electrode by constant-current oxidation or by a programmed change of current (Fig. 14), in both cases with concomitant O_2 evolution, does not show the columnar structures illustrated above. The structure is more amorphous and is associated with a higher O:Ru ratio, determined in the x-ray spectrometry experiments, than is found at the cycled material. However, these experiments always gave substantially lower O:Ru ratios than correspond to the nominal stoichiometric composition "RuO_2" taken for a thermally prepared RuO_2 specimen as standard. At electrochemically oxidized Ir, the corresponding O:Ir ratios were larger and closer to the expected "IrO_2" stoichiometry for an IrO_2 standard.

Pore structures.—Attempts were made at high SEM magnifications to detect a pore structure that might account for the large oxidation/reduction charge associated with the electrochemical behavior of oxide films developed on Ir and Ru to appreciable thicknesses (CEF values of 200-500). The columnar structures developed at Ru under certain conditions (*cf.*, Fig. 11, 12, and 13) indicate the possibility of extended pores down or between the columns. However, direct high magnification observations in the SEM were unable to distinguish fine-scale roughness from possible entrances to pores in the surface, *e.g.*, in Fig. 6. Because of this problem, several observations were made at very high magnifications by means of TEM which are described below.

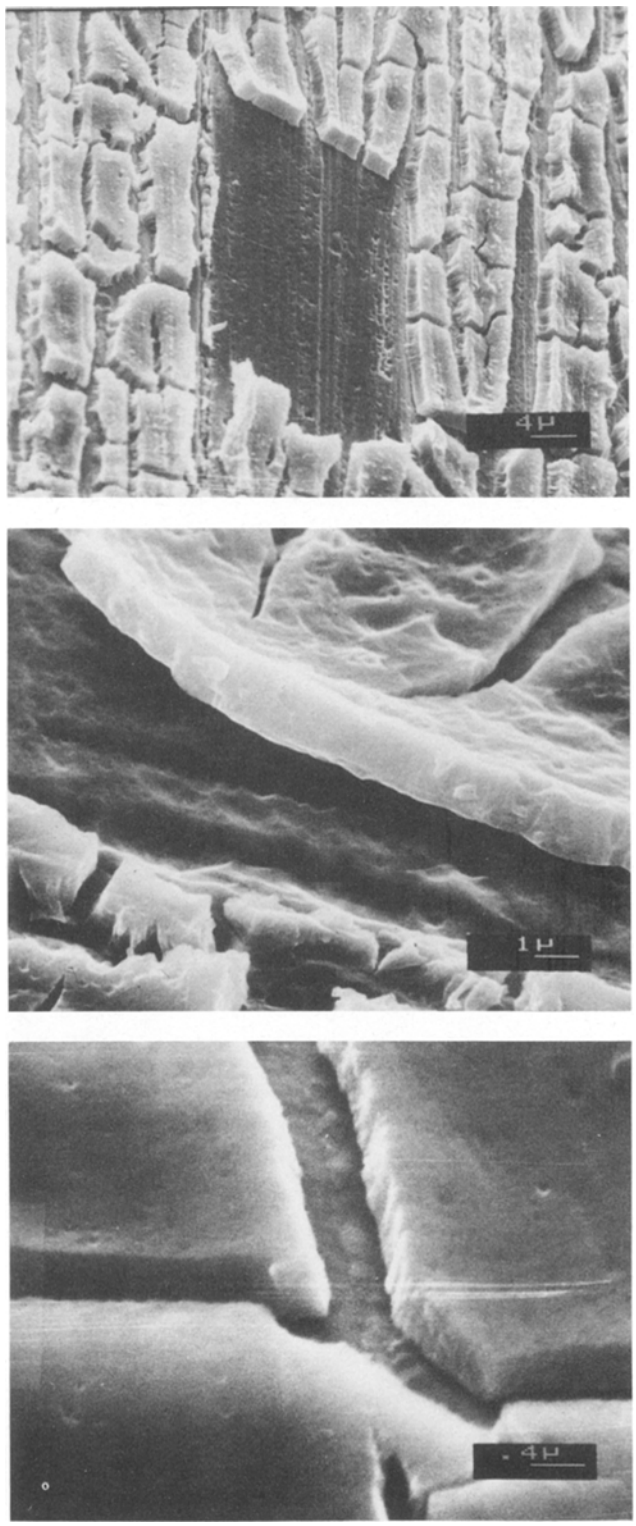

Fig. 10. SEM photos of the structure of electrochemically formed thick oxide films at an Ir electrode. (Note cracked structures not seen at Ru, and absence of outer shell layer.)

Morphologies of other deposits.—Comparison with oxide films formed in other ways is of some interest. Figure 15a shows the morphology of an RuO_2 oxide film formed thermally from a $RuCl_3$-coated electrode (Ti substrate, as with a DSA-type electrode). Figure 15b shows an oxide film developed by the cycling procedure from Ru electroplated on Au. Compared with features developed in the oxidation of bulk Ru, the oxide structure seems to be influenced mainly by the morphology of the electroplated Ru metal substrate.

Transmission electron microscopy.—During the SEM studies of the oxide films formed at Ru by potential cy-

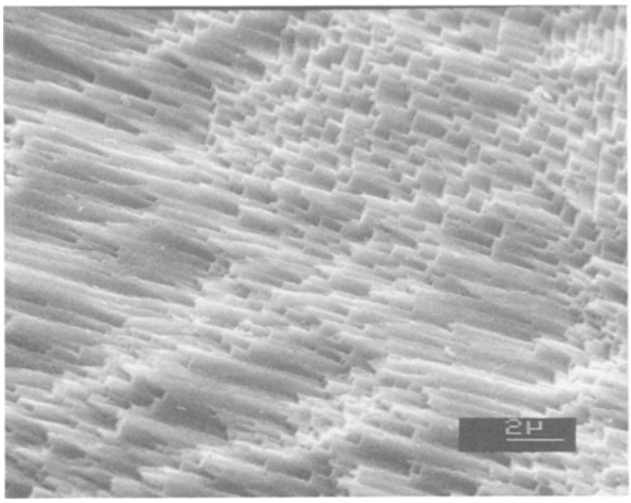

Fig. 11. SEM photo showing columnar and apparently tubular structure at electrochemically oxidized Ru electrode. Region is a fracture section.

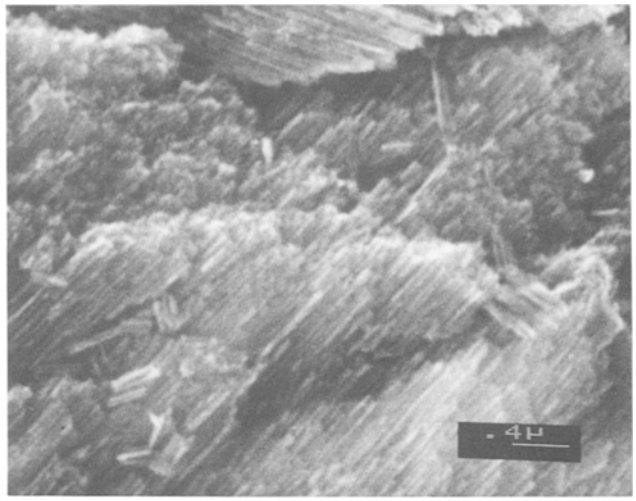

Fig. 13. Columnar structures of oxidized Ru electrode developed in relation to different grain orientations. Note detached pieces.

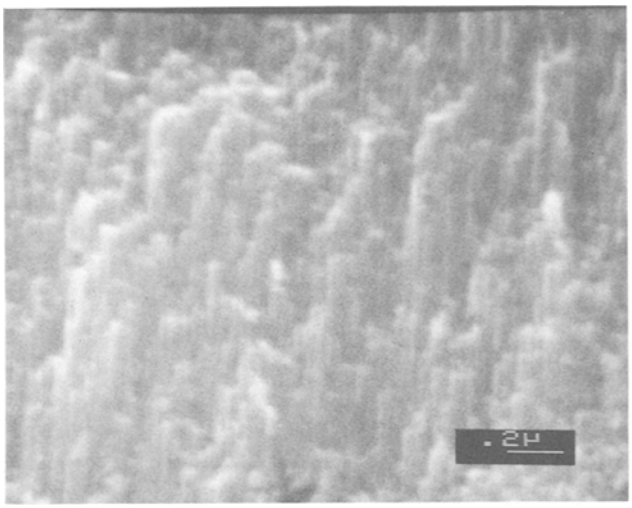

Fig. 12. Another SEM photo of the columnar structure of the oxidized Ru electrode at higher magnification and at an 86° tilt.

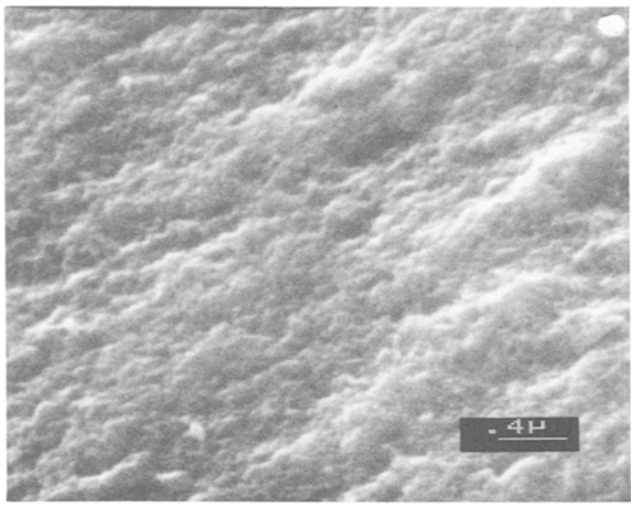

Fig. 14. SEM photo of amorphous oxide film formed at Ru under constant current oxide film formation conditions.

cling, it had been noticed that columnar structures develop in the latter material (see Fig. 5 and 11-13). It was possible to replicate the oxide surface with Formvar and, in so doing, to include some fragments of the oxide layer formed at Ru by the cycling procedure in the Formvar replica. These replicas were then examined by transmission electron microscopy. (Fig. 16a and 16b).

Figure 16a shows a TEM photograph of such a replica of the surface of the columnar film on Ru. At these high magnifications (scale of original photo 60 nm per cm), the oxide material is seen to be made up of remarkable parallel cylindrical bodies *ca.* 30 nm in diameter. Some are seen to have become separated and apparently bent around on top of other material. Details at a level of res-

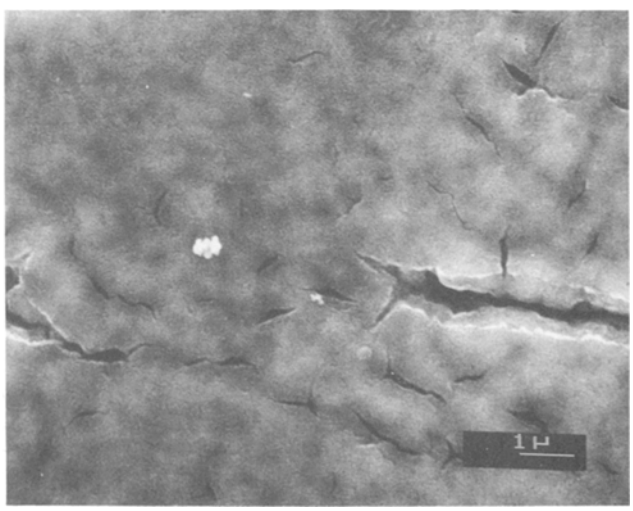

Fig. 15. a, left: SEM photo of oxide film at Ru formed thermally by decomposition of $RuCl_3$ coatings. b, right: Oxide film on Ru electroplated on Au. Film developed by the electrochemical cycling procedure.

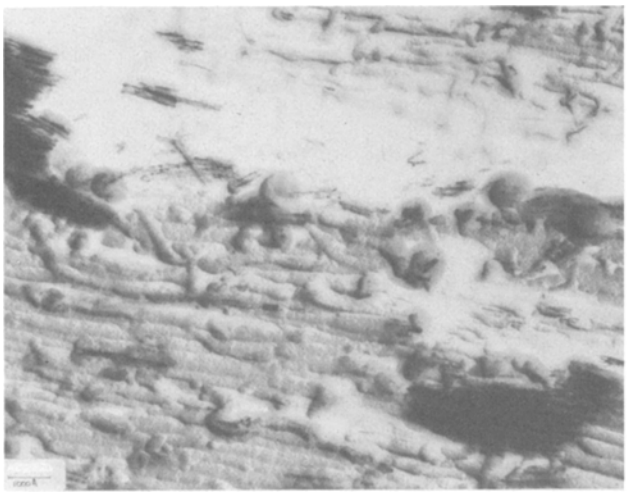

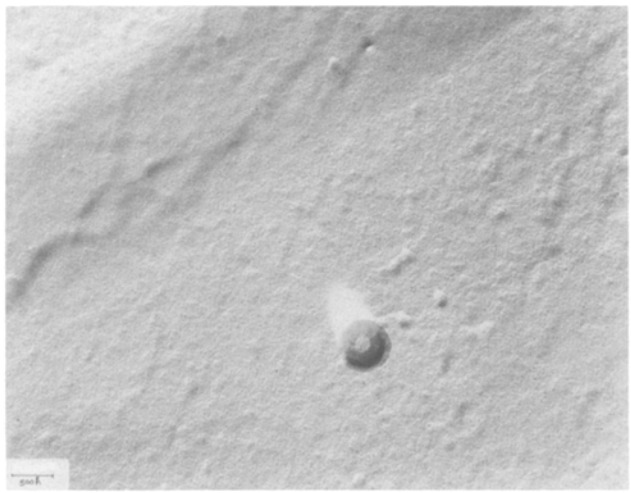

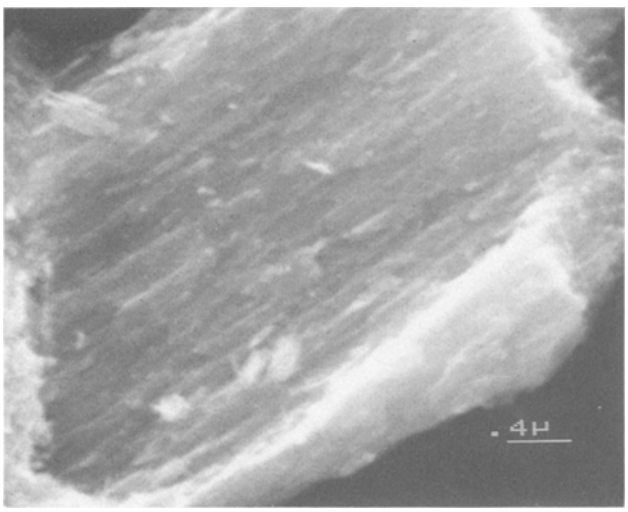

Fig. 16. a, top left: TEM photograph of the columnar structures developed at electrochemically oxidized Ru electrodes. b, top right: TEM photo of outer region of oxide film at Ru. c, left: SEM photo of a region of an actual oxide fragment trapped in the replica; see part of the TEM photo in Fig. 16a at the bottom right-hand side. In b, the circular microfeatures are clearer in the original photomicrographs than in this reproduction.

olution of < 5 nm can be detected in this photo. An SEM picture of the actual replica of the columnar material is shown in Fig. 16c.

Since the TEM photo shows the image of a replica, it is to be noted that the apparent topology is a negative of that of the actual sample fragment.[3]

The small pieces of oxide which were extracted into the replica from this region appear as the very dark areas of the TEM photograph in Fig. 16a at the lower right. The fact that the tiny oxide fragments exhibit the same columnar structure as in the replica material (*cf.* Fig. 16a) confirms the interpretation of the photomicrographs that highly oriented pores are an intrinsic part of the oxide structure. It should also be noted that the outer walls of the pores in the oxide pieces align well with the observed column edges on the remainder of the replica, demonstrating the accuracy of the replication procedure and the homogeneity of the structure. Figure 16a shows also that the channels or pores of this oxide region are of approximately 10-15 nm diam. Figure 16b is another TEM photo of a different replica of the oxidized Ru surface taken from an area where the outer layer of the oxide was still completely intact (*cf.* Fig. 4a, 4b, and 5), so that this photo shows the actual outer surface of the oxide. This photo shows many circular features having a diameter of *ca.* 10 nm. It is possible that these features are the exposed ends of some of the pores in the oxide film. The background has a fine structure on the order of 1 nm in dimensions, probably due to carbon coating the replicas.

[3]It is also to be noted that Formvar replicas of a smooth substrate surface are themselves entirely structureless, so the columnar features in Fig. 16a are not artifacts of the replication procedure. In any case, the columnar structures are seen directly under the SEM (Fig. 11-13).

An SEM photo of the oxide fragment shown in Fig. 16a is reproduced in Fig. 16c. Once again, the columnar structure is clearly seen.

In the case of Ir oxide films, these columnar structures could not be detected, and the fine structure at high magnifications seems generally like that of an amorphous material. Presumably, the apparent high area indicated by the proportionality of electrocatalytic activity for anodic Cl_2 evolution (24) to film thickness (CEF) is associated with a highly microporous structure with dimensions below those resolvable in the SEM. We refer to this as a hyperextended material.

Comparison of oxide films at Ir and Ru.—These results lend credence to the view that the high capacity for acceptance of electrochemical charge exhibited by the hydrous oxide type of materials that can be generated on Ir, Ru, and other metals [*cf.* Burke (23)] is connected with a high area pore structure which provides access for electrolyte ions and passages or chemical water channels for migration of the protons required in the oxide redox processes; these are of a remarkably reversible kind.

From an electrochemical point of view, the striking feature (18, 19, 21) of these anodically formed thick oxide films is that they exhibit a charge *vs.* potential relationship of the same kind as that of an electrochemical two-dimensional surface process, *e.g.*, submonolayer surface oxidation of Pt or underpotential deposition of metal monolayers on Au, and yet the material is demonstrably present in bulk form. In particular, for any given fractional degree of oxidation or reduction of the material, there is a corresponding reversible potential, as with an electrosorption isotherm (33) or with a three-dimensional redox system, as in the case of a redox titra-

tion. For a normal bulk phase oxide, on the contrary, there is: (*i*) an almost unique (theoretically, actually unique) single-valued potential for the formation or reduction of the oxide, and (*ii*) in a cyclic voltammetry experiment, the current *vs.* potential profiles in anodic and cathodic directions are never mirror images of each other, but correspond to processes requiring an overpotential in either direction for significant currents to pass; hence, the anodic and cathodic *i vs. V* profiles are completely asymmetric with respect to one another for other solid bulk phase materials.

While the electrochemical behavior of Ir and Ru is in some ways similar with respect to the development of thick oxide films upon potential cycling which exhibit reversible redox behavior over a wide range of potentials (wider at Ru than at Ir due to loss of conductivity (18, 31) in Ir oxide films below *ca.* 0.65V E_H, associated with reduction to a lower valence state of the Ir ions), the present work demonstrates important structural and some significant chemical differences in the films.

The principal structure difference is the development of the columnar features in the case of oxidized Ru and the retention of a hard surface on the exterior of the electrochemically generated oxide films at Ru. At Ir, neither of these features is observed and the oxide appears structurally more homogeneous (amorphous) apart from "mud cracks." Also, with Ir, no hard outer surface is retained. It may be suggested that the structures developed at Ru are the result of anodic etching accompanied by formation of a thin layer of oxide on the structures resulting from etching. This would be consistent with the appearance of substantial quantities of dissolved Ru species in solution during the film formation process under cycling or dc polarization conditions. An oxidized etched structure would also be consistent with the low O:Ru ratios found in comparison with the higher O:Ir ratios found at Ir, where the oxide film structure is visibly different. Thus, at Ru, the x-ray signals may originate relatively more from unoxidized metal contained in the film than is the case at Ir. However, the electrochemically accessible surface at the Ru material is certainly in an oxidized state, as indicated by the "reversible" cyclic voltammogram and the associated increase of CEF with cycling (Fig. 2), as well as by the difference of the features of the cyclic voltammogram compared with that for monolayer oxide formation and reduction [see Ref. (21)]

Other electrochemical differences in the properties of the films at Ru and Ir can be summarized as follows: (*i*) failure of oxide films to grow at Ir under dc potentiostatic conditions while they do grow at Ru under constant current or constant potential polarization, as well as by cycling; (*ii*) progressive increase of anodic Cl_2 or O_2 currents with oxide film thickness (CEF) at Ir but noticeably less at Ru electrodes, and (*iii*) dissolution of soluble species during oxide film formation at Ru but not significantly at Ir. Also, the change of conductivity of oxide films at Ir with potential (18, 31), referred to earlier, is to be noted.

The thick oxide film at Ir seems to be developed as a hyperextended hydrous oxide layer in which redox processes involving the Ir itself can proceed reversibly[4] and in which, through a microporous structure, other faradaic reactions, such as oxidation of Cl^-, can also occur at currents proportional to CEF (24) and hence probably to real electrochemically accessible area. However, at Ru, while similar redox processes involving some ionic states (Ru II, Ru III, Ru IV) of Ru itself can evidently take place reversibly, the body of the film structure remains inaccessible for other faradaic reactions, such as Cl_2 evolution. This, we suggest, may be due to the presence of the impervious outer layer of oxide which is seen to exist at Ru but not at Ir electrodes.

[4]Very recently, photos of thick films that can also be formed on Pt (34) have been published (35). However, the films do not show reversible redox behavior like that at Ru or Ir.

Acknowledgments

We are grateful to Mr. Dwight Craig for perceptive discussions throughout the conduct of this work. Grateful acknowledgment is also made to Continental Group, Incorporated for support of this work and for provision of an electron microscope and associated x-ray spectrometry facilities at the University of Ottawa. We are also indebted to Mr. M. Shevalier for the SEM measurements of film thicknesses on Ir at various CEF's.

Manuscript submitted Sept. 12, 1983; revised manuscript received Feb. 1, 1984. This was Paper 845 presented at the San Francisco, California, Meeting of the Society, May 8-13, 1983.

The University of Ottawa assisted in meeting the publication costs of this article.

REFERENCES

1. S. Gilman, *J. Phys. Chem.*, **67,** 1898 (1963); *ibid.*, **68,** 70 (1964).
2. V. S. Bagotzky and Y. B. Vassil'yev, *Electrochim. Acta*, **9,** 869 (1964).
3. B. E. Conway, in "Electrochemistry of Conductive Metal Oxides," Vol. B, S. Trasatti, Editor, Elsevier, Amsterdam (1980).
4. E. L. Littauer and L. L. Shrier, *Electrochim. Acta*, **11,** 127 (1966).
5. B. E. Conway and D. M. Novak, *J. Electroanal. Chem.*, **99,** 133 (1979).
6. B. E. Conway and D. M. Novak, *J. Chem. Soc., Faraday Trans. 1*, **77,** 2341 (1981); *ibid.*, **75,** 2454 (1979).
7. A. Damjanović and J. O'M. Bockris, *Electrochim. Acta*, **11,** 376 (1966).
8. J. Ord and F. C. Ho, *This Journal*, **118,** 46 (1971).
9. A. Damjanović, L. S. R. Yeh, and J. F. Wolf, *ibid*, **127,** 874 (1980); *ibid.*, **127,** 1951 (1980).
10. A. Damjanović and L. S. R. Yeh, *ibid.*, **126,** 555 (1979).
11. D. Gilroy and B. E. Conway, *Can. J. Chem.*, **46,** 875 (1968).
12. D. Gilroy, *J. Electroanal. Chem.*, **71,** 257 (1976).
13. H. Cabrera and N. F. Mott, *Rpt. Prog. Phys.*, **12,** 163 (1948-1949).
14. K. J. Vetter and J. W. Schultze, *J. Electroanal. Chem.*, **34,** 131 (1972); *ibid.*, **34,** 141 (1972).
15. P. Stonehart, H. A. Kozlowska, and B. E. Conway, *Proc. R. Soc. London, Ser. A*, **310,** 541 (1969).
16. S. Gottesfeld and B. E. Conway, *J. Chem. Soc. Faraday Trans. 1*, **69,** 1090 (1973).
17. S. Gottesfeld, *This Journal*, **127,** 1922 (1980).
18. J. Mozota and B. E. Conway, *Electrochim. Acta*, **28,** 1 (1983); *ibid.*, **28,** 9 (1983).
19. A. Capon and R. Parsons, *J. Electroanal. Chem.*, **39,** 275 (1972).
20. J. M. Otten and W. Visscher, *ibid.*, **55,** 1 (1974); *ibid.*, **55,** 13 (1974).
21. S. Hadzi-Jordanov, H. Angerstein-Kozlowska, M. Vuković, and B. E. Conway, *This Journal*, **125,** 1473 (1978).
22. D. Mitchell, D. A. J. Rand, and R. Woods, *J. Electroanal. Chem.*, **89,** 11 (1978).
23. D. N. Buckley and L. D. Burke, *J. Chem. Soc. Faraday Trans. 1*, **71,** 1447 (1975); *ibid.*, **72,** 2431 (1976).
24. B. E. Conway and J. Mozota, *This Journal*, **128,** 2142 (1981).
25. J. Vuković, H. Angerstein-Kozlowska, and B. E. Conway, *J. Appl. Electrochem.*, **12,** 193 (1982).
26. S. Gottesfeld and S. Srinivasan, *J. Electroanal. Chem.*, **86,** 89 (1978).
27. B. E. Conway, H. Angerstein-Kozlowska, W. B. A. Sharp, and E. Criddle, *Anal. Chem.*, **45,** 1331 (1973).
28. D. A. J. Rand and R. Woods, *J. Electroanal. Chem.*, **35,** 209 (1972); *ibid.*, **55,** 375 (1974).
29. J. D. McIntyre and S. Gottesfeld, *This Journal*, **126,** 742 (1979).
30. J. Augustynski, M. Koudelka, B. Sanchez, and B. E. Conway, *J. Electroanal. Chem.*, **160,** 233 (1984).
31. S. H. Glarum and J. H. Marshall, *This Journal*, **127,** 1467 (1980); see also L. D. Burke and D. P. Whelan, *J. Electroanal. Chem.*, **124,** 333 (1981).
32. J. W. Davies, J. P. S. Pringle, R. L. Graham, and F. Brown, *This Journal*, **109,** 999 (1962).
33. B. E. Conway and E. Gileadi, *Trans. Faraday Soc.*, **58,** 2493 (1962).
34. S. Shibata and M. P. Sumino, *Electrochim. Acta*, **20,** 739 (1975); see also *J. Electroanal. Chem.*, **89,** 37 (1978).
35. A. C. Chialvo, W. E. Triaca, and A. J. Arvia, *ibid.*, **146,** 93 (1983).